Neurexins control the strength and precise timing of glycinergic inhibition in the auditory brainstem

He-Hai Jiang[1,2,3], Ruoxuan Xu[1], Xiupeng Nie[1], Zhenghui Su[1], Xiaoshan Xu[1], Ruiqi Pang[4,5], Yi Zhou[4], Fujun Luo[1,2,3]*

1. Guangzhou National Laboratory, 510005, Guangzhou, Guangdong, China
2. Bioland Laboratory, 510005, Guangzhou, Guangdong, China
3. School of Basic Medical Sciences, Guangzhou Medical University, 510005, Guangzhou, Guangdong, China
4. Department of Neurobiology, School of Basic Medicine, Army Medical University, 400038, Chongqing, China
5. Advanced Institute for Brain and Intelligence, School of Medicine, Guangxi University, 530004, Nanning, China

*Correspondence author. luo_fujun@gzlab.ac.cn (F.L.)

Abstract

Neurexins play diverse functions as presynaptic organizers in various glutamatergic and GABAergic synapses. However, it remains unknown whether and how neurexins are involved in shaping functional properties of the glycinergic synapses, which mediate prominent inhibition in the brainstem and spinal cord. To address these issues, we examined the role of neurexins in a model glycinergic synapse between the principal neuron in the medial nucleus of the trapezoid body (MNTB) and the principal neuron in the lateral superior olive (LSO) in the auditory brainstem. Combining RNAscope with stereotactic injection of AAV-Cre in the MNTB of neurexin1/2/3 conditional triple knockout mice, we showed that MNTB neurons highly express all isoforms of neurexins although their expression levels vary remarkably. Selective ablation of all neurexins in MNTB neurons not only reduced the amplitude but also altered the kinetics of the glycinergic synaptic transmission at LSO neurons. The synaptic dysfunctions primarily resulted from an impaired Ca^{2+} sensitivity of release and a loosened coupling between voltage-gated Ca^{2+} channels and synaptic vesicles. Together, our current findings demonstrate that neurexins are essential in controlling the strength and temporal precision of the glycinergic synapse, which therefore corroborates the role of neurexins as key presynaptic organizers in all major types of fast chemical synapses.

Introduction

Neurexins are evolutionarily conserved synaptic adhesion molecules and their genetic mutations are highly associated with autism and schizophrenia (Gomez et al., 2021; Sudhof, 2008; 2017). In the vertebrates, neurexins are encoded by three genes Nrxn1, Nrxn2, Nrxn3, each of which contains distinct promoters for expressing longer α- and shorter β-neurexins (Ullrich et al., 1995; Ushkaryov et al., 1992). Both α- and β-neurexins are critical and non-redundant in regulating the formation and function of synapses (Anderson et al., 2015; Missler et al., 2003; Sudhof, 2017). Triple knockout (KO) of α-neurexins causes a significant decrease in the density of GABAergic but not glutamatergic synapses while producing a strong reduction in both inhibitory and excitatory synaptic transmission(Missler *et al.*, 2003). Triple KO of β-neurexins reveals a significant phenotype only in glutamatergic synapses, but not in GABAergic synapses (Anderson *et al.*, 2015). Deletion of all neurexins, including Nrxn1/2/3 α- and β-neurexins, leads to profound but strikingly distinct phenotypes in different synapses, which further points to the diverse actions of neurexins in specific neurons (Chen et al., 2017; Luo et al., 2020). Consistently, transcriptomic analysis has revealed that the expression profiles of various neurexins differ remarkably in excitatory neurons versus inhibitory neurons even among distinct subtypes of interneurons (Foldy et al., 2016; Fuccillo et al., 2015; Lukacsovich et al., 2019; Uchigashima et al., 2019). Despite the multifaceted roles of neurexins widely observed in various glutamatergic and GABAergic synapses (Boxer and Aoto, 2022; Chen *et al.*, 2017; Luo et al., 2021; Sudhof, 2017), however, it remains largely unknown how neurexins may regulate the functional properties of the glycinergic synapses, which mediate essential inhibition in the spinal cord, brainstem and retina (Assareh et al., 2023; Brill et al., 2020; Chang et al., 2023; Feng et al., 1998; Foster et al., 2015; Gomeza et al., 2003a; Gomeza et al., 2003b; Zeilhofer et al., 2012).

In the mature mammalian auditory brainstem, it is well-characterized that the principal neurons in the medial nucleus of the trapezoid body (MNTB) project glycinergic synaptic inputs to the lateral superior olive (LSO) (Fischer et al., 2019; Kotak et al., 1998; Nabekura et al., 2004; Sanes and Friauf, 2000). These synapses are robust, precise and extremely reliable even during high frequency stimulation(Krachan et al., 2017). Strong evidence has shown that the

MNTB-LSO glycinergic synapses are subject to extensive refinement during development, including transmitter type switch, the elaboration of dendrites and axonal arbors followed by synaptic pruning, to achieve exquisite control of fast inhibition(Brill *et al.*, 2020; Kim and Kandler, 2003; Kotak *et al.*, 1998; Nabekura *et al.*, 2004; Sanes and Friauf, 2000). However, the molecular mechanisms of shaping their functional characteristic remain incompletely understood.

We utilized the triple Nrxn1/2/3 conditional KO mice (Nrxn123 cTKO) (Chen *et al.*, 2017) to ablate all neurexins in MNTB principal neurons with stereotactic injection of adeno-associated -virus (AAV) expressing Cre-recombinase. Combining this with the RNAscope technique, we verified that MNTB neurons highly express various isoforms of neurexins. Selective injection of AAV-Cre, but not AAV-EGFP, successfully blocked expression of all neurexins in MNTB neurons. Functionally, pan-neurexin deletion significantly impaired both the amplitude and the kinetics of the glycinergic synaptic transmission. Surprisingly, deletion of all neurexins led to a significantly higher number of glycinergic synapses innervating the LSO and higher frequency of spontaneous neurotransmitter release. Application of low extracellular Ca^{2+} blocked the glycinergic neurotransmission of both control and neurexin-deficient synapses, but with a significant difference in its effectiveness. Moreover, treatment with EGTA, a high-affinity Ca^{2+} chelator with slow binding kinetics, caused a much stronger inhibition of neurotransmission in neurexin-deficient synapses, suggesting a significant disruption of the tight coupling between voltage-gated Ca^{2+} channels and synaptic vesicles in the MNTB-LSO glycinergic synapses.

Results

Neurexins are highly expressed in MNTB neurons

To study the role and mechanism of neurexins in the glycinergic synapse between MNTB neurons and LSO neurons, which are critical in computing sound localization in mammalian auditory brainstem (Grothe et al., 2010), we first characterized the expression of Nrxn1-3 in the principal neurons of the MNTB by fluorescent *in-situ* hybridization (FISH) using the RNAscope technique. As shown in Figure 1, MNTB neurons in wild-type (WT) mice expressed Nrxn1,

94 Nrxn2, and Nrxn3, although the expression level of each gene appeared to vary remarkably. As
95 an initial exploration, we took advantage of Nrxn123 cTKO mice that enable deletion of all
96 neurexins following the expression of Cre recombinase (Chen *et al.*, 2017), to bypass the
97 functional redundancy of different neurexins. Neuronal specific deletion of all neurexins was
98 achieved by stereotactic injection of AAV-Cre-EGFP into the MNTB at P0 (TKO). As a control,
99 AAV-EGFP was injected (Ctrl). Successful virus injection and expression of Cre recombinase
100 in MNTB neurons were confirmed by strong EGFP fluorescence (Figure 1d-e). FISH data
101 further demonstrated that the recombinase dramatically blocked the expression of all neurexins,
102 as compared to the normal expression of neurexins when EGFP was expressed (Figure 1f,
103 compared to 1b). Altogether, these data show that the glycinergic neurons in the MNTB highly
104 express various neurexin genes, which can be specifically deleted by stereotactic injection of
105 AAV-Cre in Nrxn123 cTKO mice.
106
107 **Neurexins are essential for dictating the strength and kinetics of the MNTB-LSO**
108 **glycinergic synapse**
109 Since neurexins play an essential role in orchestrating functional organization of various
110 synapses including both glutamatergic and GABAergic synapses, we hypothesize that deletion
111 of all neurexins may have a significant impact on glycinergic synapses. To test the hypothesis,
112 we sought to examine how neurexins may regulate the function of the MNTB-LSO glycinergic
113 synapse in the auditory brainstem. Because LSO neurons receive excitatory glutamatergic
114 inputs and inhibitory GABAergic/glycinergic inputs, we used a pharmacological approach to
115 isolate the glycinergic inputs. By blocking glutamatergic inputs with CNQX and AP5, we were
116 able to selectively record inhibitory postsynaptic currents (IPSCs) from LSO neurons, which
117 can be completely inhibited by strychnine, a potent glycine receptor inhibitor (Figure S1).
118 To specifically examine the role of neurexins in regulating the glycinergic synapse, we used
119 an optogenetic approach in which two AAVs, AAV-Cre-EGFP and AAV-DIO-ChR2-mCherry,
120 were co-injected in Nrxn123 cTKO mice. As a control, AAV-ChR2-EYFP was used for injection.
121 Virus injection was performed at P0 and acute slices derived from these mice were analyzed
122 at P13-14. We verified the successful expression of ChR2 by examining the fluorescence and

123 further by recording optogenetically-evoked action potentials from the soma of MNTB neurons.
124 Reliable action potential (AP) firing can be induced by single or repetitive high-frequency light
125 stimulation (Figure S1c). In control mice, optogenetic stimulation of MNTB neurons robustly
126 triggered large IPSCs recorded from LSO neurons (Figure 2a-b), which can be fully blocked by
127 strychnine (Figure S1d) and are thus purely glycinergic. In TKO mice with co-injection of Cre
128 and ChR2, however, optogenetic stimulation induced significantly smaller IPSCs (Figure 2a-b).
129 On average, we observed ~60% reduction in the peak amplitude (Figure 2b), similar to previous
130 findings at other different synapses (Chen *et al.*, 2017; Luo *et al.*, 2020). Furthermore, the
131 kinetics of IPSCs were dramatically reduced as indicated by significantly slower rise time and
132 decay time in TKO mice as compared to the control (Figure 2c-d). Together, these data strongly
133 suggest that neurexins are essential for the intact function of the glycinergic synapse.

134 To further address the physiological role of neurexins in action potential evoked
135 neurotransmission at the glycinergic synapse, we applied electric stimulation to activate
136 presynaptic fibers of MNTB neurons by placing a stimulating electrode in the midway between
137 the MNTB and the LSO. Consistent with our optogenetic approach, afferent-evoked large
138 IPSCs were predominantly glycinergic as they can also be fully blocked by strychnine (Figure
139 S1). A modest but significant decrease in synaptic strength was observed in Nrxn123 TKO mice
140 as compared to control mice (Figure 2e-f), confirming the important role of neurexins in the
141 glycinergic synapses. The modest effect of the pan-neurexin deletion on synaptic strength in
142 the MNTB-LSO synapses is likely due to the incomplete AAV virus transfection in MNTN
143 neurons. Therefore, it is likely that a small fraction of MNTB neurons may still express relatively
144 normal expression of neurexins. It is worth pointing out that extensive efforts were made to
145 optimize our virus injection protocols by adjusting the injection parameters including the needle
146 angle, virus titers, and volume. On average, it was estimated that approximately ~80% neurons
147 in the MNTB expressed GFP and thus were infected by AAV-Cre. It is also possible that other
148 sources of glycinergic inputs other than the MNTB afferents are likely to present but are
149 obscured in wild-type animals by the predominant glycinergic inputs from MNTB neurons
150 (Jalabi et al., 2013).

151 **The mechanism of neurexins for regulating the MNTB-LSO glycinergic synapse**

152 Since neurexins play multifaceted roles in regulating pre- and/or post-synaptic functions,
153 we explored the potential mechanisms by initially examining the paired-pulse ratio (PPR) of
154 IPSCs, which has been routinely used for identifying a presynaptic origin of regulation. As
155 shown in Figure 2i, IPSCs evoked by two consecutive stimuli at various intervals showed a
156 paired-pulse depression in both control and TKO mice. However, the PPRs were significantly
157 increased by deletion of neurexins (Figure 2j, s2), suggesting that neurexins are required for
158 maintaining a high release probability of the glycinergic nerve terminal.

159 We then recorded and analyzed spontaneous IPSCs from LSO neurons. Compared to the
160 control, there was no significant difference in both the amplitude and kinetics of sIPSCs (Figure
161 3a-d) in TKO mice, indicating the normal content of synaptic vesicle as well as the normal
162 function of postsynaptic glycine receptors. Surprisingly, however, we found that deletion of all
163 neurexins caused a small but significant increase in the frequency of sIPSCs (Figure 3a-b),
164 which is opposite to previous reports of either no change or decrease in the miniature frequency
165 at glutamatergic or GABAergic synapse (Chen *et al.*, 2017; Luo *et al.*, 2020). To test whether
166 the increase in sIPSC frequency may be caused by an increase in the number of glycinergic
167 synapses, we performed immunostaining of brainstem sections containing the LSO with
168 antibodies specific for GlyT2 or VGAT, synaptic markers for the glycinergic neurons. Consistent
169 with the increased frequency of sIPSCs, we found a significant increase in the density of both
170 GlyT2 (Figure 3e-f) and VGAT (Figure 3g-h) staining, suggesting more abundant glycinergic
171 terminals at the LSO of TKO mice. Together, these data show that the pan-neurexin deletion in
172 MNTB neurons has surprisingly increased the baseline glycinergic neurotransmission, which is
173 distinct from the phenotypes observed in glutamatergic and GABAergic neurons (Chen *et al.*,
174 2017; Luo *et al.*, 2021).

175 **Deletion of neurexins impairs the tight coupling between voltage-gated Ca^{2+} channels**
176 **and synaptic vesicles at the glycinergic synapse**

177 Because neurexins are shown to exert diverse impacts including specifying the function of
178 voltage-gated Ca^{2+} channels and their spatial clustering within the presynaptic active zone
179 (Chen *et al.*, 2017; Luo *et al.*, 2020; Missler *et al.*, 2003), we approached the matter by first
180 exploring the effect of pan-neurexin deletion on the calcium sensitivity of neurotransmitter

release at the MNTB-LSO synapse. We perfused the brain slice with low Ca^{2+} (0.2 mM) ACSF while recording IPSCs continuously. In both control and Nrxn123 TKO mice, the perfusion of low Ca^{2+} ACSF gradually decreased the amplitude of IPSCs (Figure 4a, c). However, the reduction rate was much faster in TKO mice such that IPSC amplitudes dropped more than 50% in TKO vs ~10% in control when extracellular [Ca^{2+}] reached to approximately 1.5 mM (Figure 4b, d). The extracellular [Ca^{2+}] blocking 50% of IPSCs were estimated as 1.1 mM and 1.5 mM respectively for control and TKO mice, which are significantly different (Figure 4e, f), suggesting that neurexins indeed are crucial for regulating calcium sensitivity of transmitter release at the glycinergic synapse.

One of the critical factors affecting the calcium sensitivity of release is the spatial distance between Ca^{2+} channels and synaptic vesicles (Eggermann et al., 2011; Luo *et al.*, 2020). Additionally, neurexins have been shown to promote tight coupling of Ca^{2+} channels with synaptic vesicle at the glutamatergic calyx of Held synapse (Luo *et al.*, 2020). Because the MNTB-LSO glycinergic synapse is similar on multiple aspects of the functional characteristics, being fast, robust, and precise, to the calyx of Held synapse, we tested whether neurexins are also required for the tight coupling of Ca^{2+} channels with synaptic vesicle. We incubated the brain slice with high-concentration EGTA-AM and continuously recorded IPSCs from individual LSO neurons. As illustrated in Figure 5, EGTA-AM treatment slightly blocked IPSCs at control synapses, suggesting the relative ineffectiveness of EGTA in interfering neurotransmitter release (Figure 5a, b). By contrast, at the neurexin-deficient synapses, EGTA-AM treatment remarkably impaired IPSCs (Figure 5c, d). On average, the blocking effects of EGTA at neurexin-deficient synapses (53.2 ± 5.4%) were much stronger than the effect at control synapses (15.6 ± 4.3%). Therefore, consistent with previous studies at the calyx of Held synapse (Luo *et al.*, 2020), our data provide further support that neurexins are key synaptic organizers for tightly clustering voltage-gated Ca^{2+} channels with synaptic vesicles at the glycinergic synapse.

Discussion

Using the MNTB-LSO synapse as a model, here we provide first assessment of the role of

210 neurexins at glycinergic synapses that mediate prominent synaptic inhibition in the brainstem.
211 Our findings in general strongly corroborate the idea that neurexins are central presynaptic
212 organizers in all major types of fast chemical synapses including glutamatergic, GABAergic and
213 glycinergic.

214 Specifically, we have shown that various neurexin genes express concurrently in these
215 glycinergic neurons but the expression level of each appears to vary significantly (Figure 1).
216 This finding is consistent with many studies in glutamatergic and GABAergic neurons, which
217 converge to show that multiple genes, isoforms, and splicing sites of neurexins normally co-
218 express in individual neurons and the expression profiles are highly cell-type specific and brain
219 region specific (Fuccillo *et al.*, 2015; Schreiner et al., 2014; Treutlein et al., 2014; Uchigashima
220 *et al.*, 2019). Distinct neurexins may interact separately and/or redundantly with diverse
221 signaling molecules to form specific molecular codes for shaping neuronal connectivity and
222 functional properties (Aoto et al., 2015; Aoto et al., 2013; Dai et al., 2019; Lin et al., 2023; Lloyd
223 et al., 2023; Sudhof, 2017). The observed differential expression of individual neurexins
224 suggests the possibility that specific isoforms may exert dominant regulatory roles in
225 neurotransmission in different synapses. For instance, compelling evidence indicates that
226 Nrxn3, arguably the best studied neurexin isoform, is selectively required for intact synaptic
227 function in the olfactory bulb GABAergic neurons (Aoto *et al.*, 2015; Trotter et al., 2023).
228 Understanding the distinct roles of each neurexin isoform in regulating glycinergic synaptic
229 transmission is crucial for future studies. Particularly noteworthy is the potential involvement of
230 Nrxn3, the most abundant isoform, in this synapse.

231 We further show that neurexins are critical in controlling the strength and precise timing of
232 the glycinergic synaptic inhibition at LSO neurons by clustering Ca^{2+} channels tightly with
233 synaptic vesicles in presynaptic release sites (Figures 2, 4 and 5). These data strongly
234 corroborate two perspectives on the function of neurexins as central presynaptic organizers.
235 First, deletion of all neurexins not only weakens the glycinergic synaptic connectivity but also
236 impairs the temporal precision of synaptic inhibition, exactly as it does at the glutamatergic
237 calyx of Held synapse (Luo *et al.*, 2020). Since both the glutamatergic calyx of Held synapse
238 and the glycinergic MNTB-LSO synapse in the auditory brainstem are extremely strong and

239 fast (Beiderbeck et al., 2018; Grothe, 2003), the orchestrating role of neurexins in controlling
240 the timing and magnitude of their synaptic transmission is therefore desirable for the auditory
241 information processing. Secondly, neurexins execute their role at the glycinergic synapse
242 mainly by tightly organizing Ca^{2+} channels within the release sites, again exactly as it does at
243 the calyx of Held synapse (Luo *et al.*, 2020). Nanodomain coupling between Ca^{2+} channels and
244 synaptic vesicles has been found in many fast central synapses and is functionally crucial for
245 increasing the efficacy and speed of neurotransmission (Eggermann *et al.*, 2011). This similar
246 role of neurexins in clustering Ca^{2+} channels tightly at presynaptic active zones of not only the
247 glutamatergic synapse but also the glycinergic synapse prompts a shared mechanism and
248 further research on the potential molecular candidates.

249 On the other hand, our data surprisingly reveal that deletion of neurexins may promote the
250 formation/maintenance of the glycinergic synapse, as evidenced by the increase in the
251 frequency of spontaneous synaptic events measured at LSO neurons as well as the increase
252 in the glycinergic synaptic density in Nrxn123 TKO mice (Figure 3). Early studies of TKOs of α-
253 neurexins or β-neurexins lead to general conclusion that neurexins are not essential for the
254 formation/maintenance of excitatory and inhibitory synapses (Anderson *et al.*, 2015; Missler *et*
255 *al.*, 2003). Moreover, deletion of all α-neurexins and β-neurexins has no impact on the
256 formation/maintenance of glutamatergic synapse (Luo *et al.*, 2020) and GABAergic synapse
257 made by somatostatin-positive interneurons (Chen *et al.*, 2017), but produces partial loss
258 (~30%) of GABAergic synapse made by parvalbumin-positive interneurons (Chen *et al.*, 2017).
259 There are several possibilities that may explain our present findings on the glycinergic synapse.
260 First, the most parsimonious explanation would be that neurexins play contradictory dual roles
261 at the glycinergic synapse: orchestrate the synchronized synaptic transmission by promoting
262 tight coupling of Ca^{2+} channels with synaptic vesicles at the presynaptic active zone; restrict
263 the formation of weaker synapse or spontaneous transmission. Another well-established
264 example of synaptic protein with dual functions in synaptic transmission is synaptotagmin 1,
265 which acts as a calcium sensor to trigger synchronous release while clamps and restricts
266 spontaneous fusion of vesicles on the other hand(Sudhof, 2013). It is worthy of note that
267 synaptotagmin can specifically interact with neurexins (Hata et al., 1993). Second, deletion of

268 neurexins impairs the strength of the MNTB-LSO synapse, which may indirectly interfere with
269 synaptic elimination process and therefore lead to an increase in synaptic density. Third, the
270 more abundant glycinergic synapses may arise from the developmental compensation of
271 synapse formation by other sources of glycinergic neurons (Jalabi *et al.*, 2013). Strong
272 reduction in the strength of the MNTB-LSO synapse caused by selective deletion of neurexins
273 may shift the winner of synaptic competition toward other parallel but much weaker glycinergic
274 inputs in normal animals.
275

276 **Methods**

277 **Mouse breeding and virus injection.**

278 All animal experiments were approved by the Institutional Animal Care and Use Committee at
279 Bioland Laboratory, Guangzhou National Laboratory, Guangzhou, China. Transgenic Nrxn123
280 cTKO mice of either sex were used for all experiments. Mice were housed at room
281 temperature on a 12 h light–dark cycle (7:00 to 19:00, light) with food and water freely
282 available.

283 To delete neurexins in MNTB neurons, we injected P0 mice with AAV2/9-hSyn-EGFP-
284 P2A-Cre-WPRE-hGH-Poly (Cat:PT-0156, BrainVTA Co., China). Mice were anesthetized on
285 ice and immediately transferred to a stereotaxic apparatus (RWD Life Technology, China).
286 Injection was achieved by connecting a glass pipette with tip diameter 20-30 μm to Nanoject
287 III programmable nanoliter injector (Drummond Scientific Company, USA). To enhance virus
288 infection efficiency, we decreased the dosage per injection while increasing the frequency of
289 injections. Additionally, we ensured the pipette remained immobilized for 20-30 seconds to
290 guarantee virus absorption at injection sites. As a result of this strategy, we estimated that the
291 vast majority of MNTB neurons were inoculated by AAVs. Bilateral injections were performed
292 at the following coordinates: AP from the most rostral point: 5.61 mm, ML: ±0.27 mm, DV:
293 3.58 mm. For optogenetics experiments, we injected 200 nl (AAV2/9-hSyn-EGFP-P2A-Cre-
294 WPRE-hGH-PolyA and AAV2/9-EF1α-DIO-hChR2(H134R)-mCherry-WPRE-hGH-Poly, 1:1,
295 Cat: PT-0002, BrainVTA Co., China) or 100 nl of AAV2/9-hSyn-hChR2(H123R)-EYFP-WPRE-
296 hGH-PolyA (Cat: PT-1317, BrainVTA Co., China) into each-side MNTB. P13-14 mice of either

sex were used for most experiments including electrophysiology, FISH and immunohistochemistry.

Acute slice preparation for electrophysiology

Coronal brain slices containing both the MNTB and LSO were prepared similarly as described previously. In brief, mice of P13-14 were decapitated; brains were rapidly isolated and fixed on the cutting platform a vibratome (VT1200s; Leica, USA), which was immersed in oxygenated cold ACSF containing (in mM): 119 NaCl, 26 $NaHCO_3$, 10 glucose, 1.25 NaH_2PO_4, 2.5 KCl, 0.05 $CaCl_2$, 3 $MgCl_2$, 2 Na-pyruvate, and 0.5 ascorbic acid, pH 7.4. Transverse slices of 250 μm were sectioned and transferred into a beaker with bubbled ACSF containing (in mM): 119 NaCl, 26 NaHCO3, 10 glucose, 1.25 NaH_2PO_4, 2.5 KCl, 2 $CaCl_2$, 1 $MgCl_2$, 2 Na-pyruvate, and 0.5 ascorbic acid, pH 7.4. Slices were recovered at 35°C for 30 minutes, and stored at room temperature (~21-23°C) for experiments.

Whole-cell voltage-clamped recordings

Whole-cell voltage-clamped recordings were made from visually identified LSO neurons in acute brain slices using an Axopatch 700B amplifier (Molecular Devices, USA) and pClamp 11 software (Molecular Devices, USA). Patch pipettes were pulled from borosilicate glass capillaries using a two-stage vertical puller (PC-100, Narashige, Japan). Pipette resistance was 4-6 MΩ when filled with an internal solution containing (in mM): 145 K-gluconate, 6 KCl, 10 HEPES, 3 Na_2-phosphocreatine, 4 Mg-ATP, 0.3 Na_2-GTP, 0.2 EGTA, 2 Qx-314; pH 7.2 with KOH. With the extracellular [Cl^-] of 133 mM and a temperature of 22°, the equilibrium potential of the Cl^- was approximately −78.8 mV. In voltage-clamp configuration, IPSCs were recorded by holding cells at 10 mV in ACSF containing CNQX (20 μM), D-AP5 (50 μM), to block AMPA, NMDA receptors, respectively. For some experiments, 2 μM strychnine, a potent glycine receptor antagonist, was added to ACSF to verify that IPSCs recorded at LSO neurons are glycinergic. Membrane potentials were not corrected for liquid junction potential. Electrical fiber stimulation was performed using a concentric bipolar electrode (CBAEB75, FHC Inc, USA) positioned medially to the LSO and MNTB. Short pulses (0.1 ms) were

delivered via an isolated stimulator (Model 2100; A-M Systems, USA). For optogenetics, a light simulation of 5 ms was delivered by LED (pE-300 white, CoolLED, UK).

Whole-cell current-clamp recordings

Whole-cell current-clamped recordings were performed similarly as voltage-clamped recordings, except that the internal solution did not contain Qx-314. Action potentials at MNTB neurons were recorded by holding the membrane potential at approximately −70 mV. For optogenetics, a light simulation of 5 ms was delivered by LED (pE-300 white, CoolLED, UK).

RNAscope fluorescent in-situ hybridization (FISH) and immunohistochemistry

Mice were anesthetized and perfused at speed of 1ml/min with 1×PBS for 10 min followed by 4% paraformaldehyde (PFA) for 10 min. Brains were removed and stored in 4% PFA overnight at 4C. After going through a 10%, 20%, and 30% sucrose gradient for cryo-protection, the tissue was embedded in OCT (Cat：14020108926, Leica) and rapidly frozen on dry ice. Transverse sections at 16 μm were cut at -20 °C using a cryostat (CM3050-S, Leica) and mounted directly on Superfrost Plus slides (Cat: PRO-04, Matsunami Platinum Pro). FISH and immunohistochemistry were performed using the RNAscope multiplex platform (Multiplex Reagent Kit, Cat: 323100; Co-detection ancillary Kit, Cat: 323180, Advanced Cell Diagnostics) following the manufacturer's instructions. RNA probes for Nrxn1, Nrxn2, and Nrxn3 (Cat: 461511-C3, 533531-C2, 505431 respectively, Advanced Cell Diagnostics) and primary antibody against VGluT1 (guinea pig, polyclonal, 1:500, Millipore) were used. Secondary antibodies were Alexa Fluor conjugates (1:400; Thermo Fisher). Samples were mounted with a Vectashield hard-set antifade mounting medium (Cat: H-1500, Vector Laboratories). Images were acquired using Zeiss LSM800 confocal microscope with a 63x oil-immersion objective (1.4 numerical aperture) or OLYMPUS IXplore SpinSR confocal microscope with a 60x oil-immersion objective (1.5 numerical aperture). Image analysis were performed using Zeiss 2.6, cellSens Dimension 3.2 and Image J.

Pharmacological manipulations

To estimate the calcium sensitivity of neurotransmitter release, we perfused the slice with ACSF containing low Ca^{2+} (0.2 mM) and continuously recorded eIPSC. EC_{50} of Ca^{2+} sensitivity was determined using a sigmoidal function (Y = Min + (Max-Min)/(1+10ˆ((LogEC_{50}-X) ∗ n))), where Y represents IPSC amplitude, X denotes the calculated extracellular Ca^{2+} concentration, Min refers to the minimal amplitude, Max represents the maximum amplitude. To estimate the spatial relationship between voltage-gated Ca^{2+} channels and synaptic vesicles, we perfused the slice with ACSF containing 20 μM EGTA-AM for 25~30 mins while continuously recording eIPSC. The blocking effect of EGTA on eIPSCs were evaluated by comparing eIPSCs before and after EGTA treatment.

Statistical analysis

Data were analyzed in the IgorPro (Version 8) and GraphPad Prism 9 software. Summary of data was displayed as mean ± SEM. Statistical analysis was performed using Student's *t* test, two-way ANOVA, and Mann-Whitney U test. Significance of difference was accepted at $P < 0.05$.

References

Anderson, G.R., Aoto, J., Tabuchi, K., Foldy, C., Covy, J., Yee, A.X., Wu, D., Lee, S.J., Chen, L., Malenka, R.C., and Sudhof, T.C. (2015). beta-Neurexins Control Neural Circuits by Regulating Synaptic Endocannabinoid Signaling. Cell *162*, 593-606. 10.1016/j.cell.2015.06.056.

Aoto, J., Foldy, C., Ilcus, S.M., Tabuchi, K., and Sudhof, T.C. (2015). Distinct circuit-dependent functions of presynaptic neurexin-3 at GABAergic and glutamatergic synapses. Nat Neurosci *18*, 997-1007. 10.1038/nn.4037.

Aoto, J., Martinelli, D.C., Malenka, R.C., Tabuchi, K., and Sudhof, T.C. (2013). Presynaptic neurexin-3 alternative splicing trans-synaptically controls postsynaptic AMPA receptor trafficking. Cell *154*, 75-88. 10.1016/j.cell.2013.05.060.

Assareh, N., Fenech, C., Power, R., Uddin, M.N., Otsu, Y., and Aubrey, K.R. (2023). Bidirectional Modulation of Nociception by GlyT2(+) Neurons in the Ventrolateral Periaqueductal Gray. eNeuro *10*. 10.1523/ENEURO.0069-23.2023.

Beiderbeck, B., Myoga, M.H., Muller, N.I.C., Callan, A.R., Friauf, E., Grothe, B., and Pecka, M. (2018). Precisely timed inhibition facilitates action potential firing for spatial coding in the auditory brainstem. Nat Commun *9*, 1771. 10.1038/s41467-018-04210-y.

Boxer, E.E., and Aoto, J. (2022). Neurexins and their ligands at inhibitory synapses. Front Synaptic Neurosci *14*, 1087238. 10.3389/fnsyn.2022.1087238.

390 Brill, S.E., Maraslioglu, A., Kurz, C., Kramer, F., Fuhr, M.F., Singh, A., and Friauf, E. (2020). Glycinergic
391 Transmission in the Presence and Absence of Functional GlyT2: Lessons From the Auditory
392 Brainstem. Front Synaptic Neurosci *12*, 560008. 10.3389/fnsyn.2020.560008.
393 Chang, Z., Skach, J., and Kam, K. (2023). Inhibitory subpopulations in preBotzinger Complex play
394 distinct roles in modulating inspiratory rhythm and pattern. bioRxiv. 10.1101/2023.08.07.552303.
395 Chen, L.Y., Jiang, M., Zhang, B., Gokce, O., and Sudhof, T.C. (2017). Conditional Deletion of All
396 Neurexins Defines Diversity of Essential Synaptic Organizer Functions for Neurexins. Neuron *94*,
397 611-625 e614. 10.1016/j.neuron.2017.04.011.
398 Dai, J., Aoto, J., and Sudhof, T.C. (2019). Alternative Splicing of Presynaptic Neurexins Differentially
399 Controls Postsynaptic NMDA and AMPA Receptor Responses. Neuron *102*, 993-1008 e1005.
400 10.1016/j.neuron.2019.03.032.
401 Eggermann, E., Bucurenciu, I., Goswami, S.P., and Jonas, P. (2011). Nanodomain coupling between
402 Ca(2)(+) channels and sensors of exocytosis at fast mammalian synapses. Nat Rev Neurosci *13*, 7-
403 21. 10.1038/nrn3125.
404 Feng, G., Tintrup, H., Kirsch, J., Nichol, M.C., Kuhse, J., Betz, H., and Sanes, J.R. (1998). Dual
405 requirement for gephyrin in glycine receptor clustering and molybdoenzyme activity. Science *282*,
406 1321-1324. 10.1126/science.282.5392.1321.
407 Fischer, A.U., Muller, N.I.C., Deller, T., Del Turco, D., Fisch, J.O., Griesemer, D., Kattler, K., Maraslioglu,
408 A., Roemer, V., Xu-Friedman, M.A., et al. (2019). GABA is a modulator, rather than a classical
409 transmitter, in the medial nucleus of the trapezoid body-lateral superior olive sound localization
410 circuit. J Physiol *597*, 2269-2295. 10.1113/JP277566.
411 Foldy, C., Darmanis, S., Aoto, J., Malenka, R.C., Quake, S.R., and Sudhof, T.C. (2016). Single-cell
412 RNAseq reveals cell adhesion molecule profiles in electrophysiologically defined neurons. Proc
413 Natl Acad Sci U S A *113*, E5222-5231. 10.1073/pnas.1610155113.
414 Foster, E., Wildner, H., Tudeau, L., Haueter, S., Ralvenius, W.T., Jegen, M., Johannssen, H., Hosli, L.,
415 Haenraets, K., Ghanem, A., et al. (2015). Targeted ablation, silencing, and activation establish
416 glycinergic dorsal horn neurons as key components of a spinal gate for pain and itch. Neuron *85*,
417 1289-1304. 10.1016/j.neuron.2015.02.028.
418 Fuccillo, M.V., Foldy, C., Gokce, O., Rothwell, P.E., Sun, G.L., Malenka, R.C., and Sudhof, T.C. (2015).
419 Single-Cell mRNA Profiling Reveals Cell-Type-Specific Expression of Neurexin Isoforms. Neuron
420 *87*, 326-340. 10.1016/j.neuron.2015.06.028.
421 Gomez, A.M., Traunmuller, L., and Scheiffele, P. (2021). Neurexins: molecular codes for shaping
422 neuronal synapses. Nat Rev Neurosci *22*, 137-151. 10.1038/s41583-020-00415-7.
423 Gomeza, J., Hulsmann, S., Ohno, K., Eulenburg, V., Szoke, K., Richter, D., and Betz, H. (2003a).
424 Inactivation of the glycine transporter 1 gene discloses vital role of glial glycine uptake in
425 glycinergic inhibition. Neuron *40*, 785-796. 10.1016/s0896-6273(03)00672-x.
426 Gomeza, J., Ohno, K., Hulsmann, S., Armsen, W., Eulenburg, V., Richter, D.W., Laube, B., and Betz,
427 H. (2003b). Deletion of the mouse glycine transporter 2 results in a hyperekplexia phenotype and
428 postnatal lethality. Neuron *40*, 797-806. 10.1016/s0896-6273(03)00673-1.
429 Grothe, B. (2003). New roles for synaptic inhibition in sound localization. Nat Rev Neurosci *4*, 540-
430 550. 10.1038/nrn1136.
431 Grothe, B., Pecka, M., and McAlpine, D. (2010). Mechanisms of sound localization in mammals.
432 Physiol Rev *90*, 983-1012. 10.1152/physrev.00026.2009.
433 Hata, Y., Davletov, B., Petrenko, A.G., Jahn, R., and Sudhof, T.C. (1993). Interaction of synaptotagmin

with the cytoplasmic domains of neurexins. Neuron *10*, 307-315. 10.1016/0896-6273(93)90320-q.

Jalabi, W., Kopp-Scheinpflug, C., Allen, P.D., Schiavon, E., DiGiacomo, R.R., Forsythe, I.D., and Maricich, S.M. (2013). Sound localization ability and glycinergic innervation of the superior olivary complex persist after genetic deletion of the medial nucleus of the trapezoid body. J Neurosci *33*, 15044-15049. 10.1523/JNEUROSCI.2604-13.2013.

Kim, G., and Kandler, K. (2003). Elimination and strengthening of glycinergic/GABAergic connections during tonotopic map formation. Nat Neurosci *6*, 282-290. 10.1038/nn1015.

Kotak, V.C., Korada, S., Schwartz, I.R., and Sanes, D.H. (1998). A developmental shift from GABAergic to glycinergic transmission in the central auditory system. J Neurosci *18*, 4646-4655. 10.1523/JNEUROSCI.18-12-04646.1998.

Krachan, E.G., Fischer, A.U., Franke, J., and Friauf, E. (2017). Synaptic reliability and temporal precision are achieved via high quantal content and effective replenishment: auditory brainstem versus hippocampus. J Physiol *595*, 839-864. 10.1113/JP272799.

Lin, P.Y., Chen, L.Y., Jiang, M., Trotter, J.H., Seigneur, E., and Sudhof, T.C. (2023). Neurexin-2: An inhibitory neurexin that restricts excitatory synapse formation in the hippocampus. Sci Adv *9*, eadd8856. 10.1126/sciadv.add8856.

Lloyd, B.A., Han, Y., Roth, R., Zhang, B., and Aoto, J. (2023). Neurexin-3 subsynaptic densities are spatially distinct from Neurexin-1 and essential for excitatory synapse nanoscale organization in the hippocampus. Nat Commun *14*, 4706. 10.1038/s41467-023-40419-2.

Lukacsovich, D., Winterer, J., Que, L., Luo, W., Lukacsovich, T., and Foldy, C. (2019). Single-Cell RNA-Seq Reveals Developmental Origins and Ontogenetic Stability of Neurexin Alternative Splicing Profiles. Cell Rep *27*, 3752-3759 e3754. 10.1016/j.celrep.2019.05.090.

Luo, F., Sclip, A., Jiang, M., and Sudhof, T.C. (2020). Neurexins cluster Ca(2+) channels within the presynaptic active zone. EMBO J *39*, e103208. 10.15252/embj.2019103208.

Luo, F., Sclip, A., Merrill, S., and Sudhof, T.C. (2021). Neurexins regulate presynaptic GABAB-receptors at central synapses. Nat Commun *12*, 2380. 10.1038/s41467-021-22753-5.

Missler, M., Zhang, W., Rohlmann, A., Kattenstroth, G., Hammer, R.E., Gottmann, K., and Sudhof, T.C. (2003). Alpha-neurexins couple Ca2+ channels to synaptic vesicle exocytosis. Nature *423*, 939-948. 10.1038/nature01755.

Nabekura, J., Katsurabayashi, S., Kakazu, Y., Shibata, S., Matsubara, A., Jinno, S., Mizoguchi, Y., Sasaki, A., and Ishibashi, H. (2004). Developmental switch from GABA to glycine release in single central synaptic terminals. Nat Neurosci *7*, 17-23. 10.1038/nn1170.

Sanes, D.H., and Friauf, E. (2000). Development and influence of inhibition in the lateral superior olivary nucleus. Hear Res *147*, 46-58. 10.1016/s0378-5955(00)00119-2.

Schreiner, D., Nguyen, T.M., Russo, G., Heber, S., Patrignani, A., Ahrne, E., and Scheiffele, P. (2014). Targeted combinatorial alternative splicing generates brain region-specific repertoires of neurexins. Neuron *84*, 386-398. 10.1016/j.neuron.2014.09.011.

Sudhof, T.C. (2008). Neuroligins and neurexins link synaptic function to cognitive disease. Nature *455*, 903-911. 10.1038/nature07456.

Sudhof, T.C. (2013). Neurotransmitter release: the last millisecond in the life of a synaptic vesicle. Neuron *80*, 675-690. 10.1016/j.neuron.2013.10.022.

Sudhof, T.C. (2017). Synaptic Neurexin Complexes: A Molecular Code for the Logic of Neural Circuits. Cell *171*, 745-769. 10.1016/j.cell.2017.10.024.

Treutlein, B., Gokce, O., Quake, S.R., and Sudhof, T.C. (2014). Cartography of neurexin alternative splicing mapped by single-molecule long-read mRNA sequencing. Proc Natl Acad Sci U S A *111*, E1291-1299. 10.1073/pnas.1403244111.

Trotter, J.H., Wang, C.Y., Zhou, P., Nakahara, G., and Sudhof, T.C. (2023). A combinatorial code of neurexin-3 alternative splicing controls inhibitory synapses via a trans-synaptic dystroglycan signaling loop. Nat Commun *14*, 1771. 10.1038/s41467-023-36872-8.

Uchigashima, M., Cheung, A., Suh, J., Watanabe, M., and Futai, K. (2019). Differential expression of neurexin genes in the mouse brain. J Comp Neurol *527*, 1940-1965. 10.1002/cne.24664.

Ullrich, B., Ushkaryov, Y.A., and Sudhof, T.C. (1995). Cartography of neurexins: more than 1000 isoforms generated by alternative splicing and expressed in distinct subsets of neurons. Neuron *14*, 497-507. 10.1016/0896-6273(95)90306-2.

Ushkaryov, Y.A., Petrenko, A.G., Geppert, M., and Sudhof, T.C. (1992). Neurexins: synaptic cell surface proteins related to the alpha-latrotoxin receptor and laminin. Science *257*, 50-56. 10.1126/science.1621094.

Zeilhofer, H.U., Wildner, H., and Yevenes, G.E. (2012). Fast synaptic inhibition in spinal sensory processing and pain control. Physiol Rev *92*, 193-235. 10.1152/physrev.00043.2010.

ACKNOWLEDGEMENTS

We thank Dr. B. Zhang (Shenzhen Bay Laboratory) for helpful comments on the manuscript. This study was supported by grants from the National Natural Science Foundation of China (31970914 to F.L.; 32171001, 32371050 to Y.Z.).

AUTHOR CONTRIBUTIONS

Conceptualization, F.L.; Experiments, H.J., R.X., X.N., Z.S., X.X., R. P.; Data analysis, H.J., R.X., X.N., Z.S., X.X., Y.Z, F.L.; Writing – Original Draft, F.L.; Writing – Review & Editing, H.J, Y.Z, F.L.

DECLARATION OF INTEREST

The authors declare no competing financial interests.

Figure legends

Fig.1 Neurexins are highly expressed in MNTB neurons. (**a**) Immunohistochemistry and RNAscope FISH showing expression of various isoforms of neurexins in the MNTB, which make glycinergic synapses with LSO neurons (**b**) Summary of expression of various isoforms of neurexins in the MNTB of WT mice. Nrxn1 (n = 29), Nrxn2 (n = 29), P = 0.0001; Nrxn1 (n = 29), Nrxn3 (n = 24), P = 0.0001; Nrxn2 (n = 29), Nrxn3 (n = 24), P = 0.0001. (**c**) Diagram of auditory brainstem and virus injection in Nrxn123 cTKO mice. (**d**) Representative images of Nrxn3 FISH in the MNTB of mice injected with AAV-EGFP or AAV-Cre-EGFP. Scale bar: 50 μm. (**e**) Selected ROI in high magnification showing Nrxn3 FISH in MNTB neurons expressing EGFP or Cre-EGFP. Scale bar: 10 μm. (**f**) Summary of expression of various neurexins in the MNTB of Nrxn123 cTKO mice injected with AAV-EGFP and AAV-Cre-EGFP. Nrxn1: EGFP (n = 9), Cre (n = 19), P = 0.0053; Nrxn2: EGFP (n = 8), Cre (n = 14), P = 0.0038; Nrxn3: EGFP (n = 9), Cre (n = 14), P = 0.0016.

Data are means ± SEM. Number of sections analyzed are indicated in the bars (**b**, **f)**; Statistical differences were assessed by Student's t test. (**P < 0.01, ***P < 0.001). Source data are provided as a Source Data file.

Figure 2 Deletion of neurexins reduces the strength and kinetics of glycinergic synapse. (**a**) Representative IPSC traces of LSO neurons evoked by optogenetic stimulation of ChR2 expressed in MNTB neurons. (**b-d**) Summary of IPSC amplitude, rise time, and decay time constant. Ctrl (n = 15), TKO (n = 11), P = 0.0119, P = 0.0004, P = 0.002. unpaired two-sided t-test. (**e-h**) Same as a-d, except that IPSCs were evoked by afferent fiber stimulation. Ctrl (n = 15), TKO (n = 16), P = 0.0267, P = 0.152, P = 0.241. (**i**) Representative IPSCs traces of LSO neurons evoked by a pair of fiber stimulation at 50 ms interval. (**j**) Summary of paired-pulse ratio (PPR) of IPSCs in relationship to different paired pulse intervals. Ctrl (n = 12), TKO (n = 12), P < 0.0001, two-way ANOVA.

Data are means ± SEM. Number of neuron are indicated in the bars (**b-d**, **f-h**) or graph (**j**)**.** Statistical differences were assessed by Student's t test or two-way ANOVA test. (*P < 0.05,

539 **P < 0.01, ***P < 0.001).

540 **Figure 3 Deletion of neurexins increases sIPSC frequency and glycinergic synapse**
541 **density of LSO neurons.** (**a**) Representative sIPSC traces of LSO neurons. (**b**) Summary of
542 sIPSC amplitude and frequency. Ctrl (n = 14), TKO (n = 9), P = 0.057, P = 0.015, unpaired two-
543 sided t-test. (**c**) Representative sIPSC waveforms of LSO neurons. (**d**) Summary of sIPSC rise
544 time and decay time constant. Ctrl (n = 14), TKO (n = 9), P = 0.376, P = 0.82, unpaired two-
545 sided t-test. (**e**) Representative confocal microscopy images of MNTB-LSO-containing
546 brainstem slice with specific labeling of GlyT2 (red) and EGFP (green) from both control and
547 Nrxn123 TKO mice at P14. Scale bar, 10 μm. (**f**) Summary of glycinergic synaptic density
548 quantified by GlyT2 immunostaining. Ctrl (n = 42), TKO (n = 42), P = 0.0001, unpaired two-
549 sided t-test. (**g-h**), Same as (**e-f**) except for specific labeling of VGAT (red) and EGFP (green).
550 Ctrl (n = 42), TKO (n = 42), P = 0.0047, unpaired two-sided t-test.

551 Data are means ± SEM. Number of neuron or sections/animals for immunostaining are
552 indicated in the bars (**b**, **d**, **f** and **h**). Statistical differences were assessed by Student's t test.
553 (*P < 0.05, **P < 0.01, ***P < 0.001). Source data are provided as a Source Data file.

554 **Figure 4 Deletion of neurexins increases the Ca^{2+} sensitivity of release at the glycinergic**
555 **synapse.** (**a**) Representative time courses of IPSC amplitudes for individual LSO neurons of
556 control mice during the perfusion of low Ca^{2+} ACSF. (**b**) Representative IPSC traces of control
557 mice before and during low Ca^{2+} perfusion at the indicated points in **a**. (**c** & **d**) Same as **a** & **b**,
558 except of TKO mice. (**e**) Summary of normalized IPSC amplitudes plotted against the calculated
559 extracellular Ca^{2+} concentration for control and TKO mice. Ctrl (n = 7), TKO (n = 9), P = 0.0311
560 for 0.92 mM Ca^{2+}, P = 0.0104 for 1.10 mM Ca^{2+}, P = 0.0208 for 1.28 mM Ca^{2+}, P = 0.0067 for
561 1.46 mM Ca^{2+}, P = 0.0007 for 1.64 mm Ca^{2+}, unpaired two-sided t-test. (**f**) Summary of EC_{50} of
562 Ca^{2+} for half-blocking of IPSCs and the blocking effect of 0.2 mM Ca^{2+} on IPSC amplitude. Ctrl
563 (n = 7), TKO (n = 9), P = 0.0139, P = 0.3985, unpaired two-sided t-test.

564 Data are means ± SEM. Number of neuron are indicated in the graph (**e**) or bars (**f**). Statistical
565 differences were assessed by Student's t test. (*P < 0.05, **P < 0.01, ***P < 0.001). Source
566 data are provided as a Source Data file.

567

568 **Figure 5 Deletion of neurexins increases the blocking effect of EGTA on glycinergic**
569 **IPSCs.** (**a**) Representative time courses of IPSC amplitudes for individual LSO neurons of
570 control mice during the treatment of high concentration of EGTA-AM. (**b**) Representative IPSC
571 traces of control mice before and after EGTA. (**c, d**) Same as a, b, except of TKO mice. (**e**)
572 Summary of IPSC amplitude before and after EGTA treatment of control mice. Ctrl (n = 7), TKO
573 (n = 7), P = 0.0201, paired two-sided t-test. (**f**) Summary of IPSC amplitude before and after
574 EGTA treatment of TKO mice. Ctrl (n = 7), TKO (n = 7), P = 0.0123, paired two-sided t-test. (**g**)
575 Summary of the blocking percentage of IPSCs by EGTA. Ctrl (n = 7), TKO (n = 7), P = 0.0001,
576 unpaired two-sided t-test.

577 Data are means ± SEM. Number of neuron are indicated in the bars (**e** to **g**). Statistical
578 differences were assessed by Student's t test. (*P < 0.05, ***P < 0.001). Source data are
579 provided as a Source Data file.

580

581

582 **Figure 1**

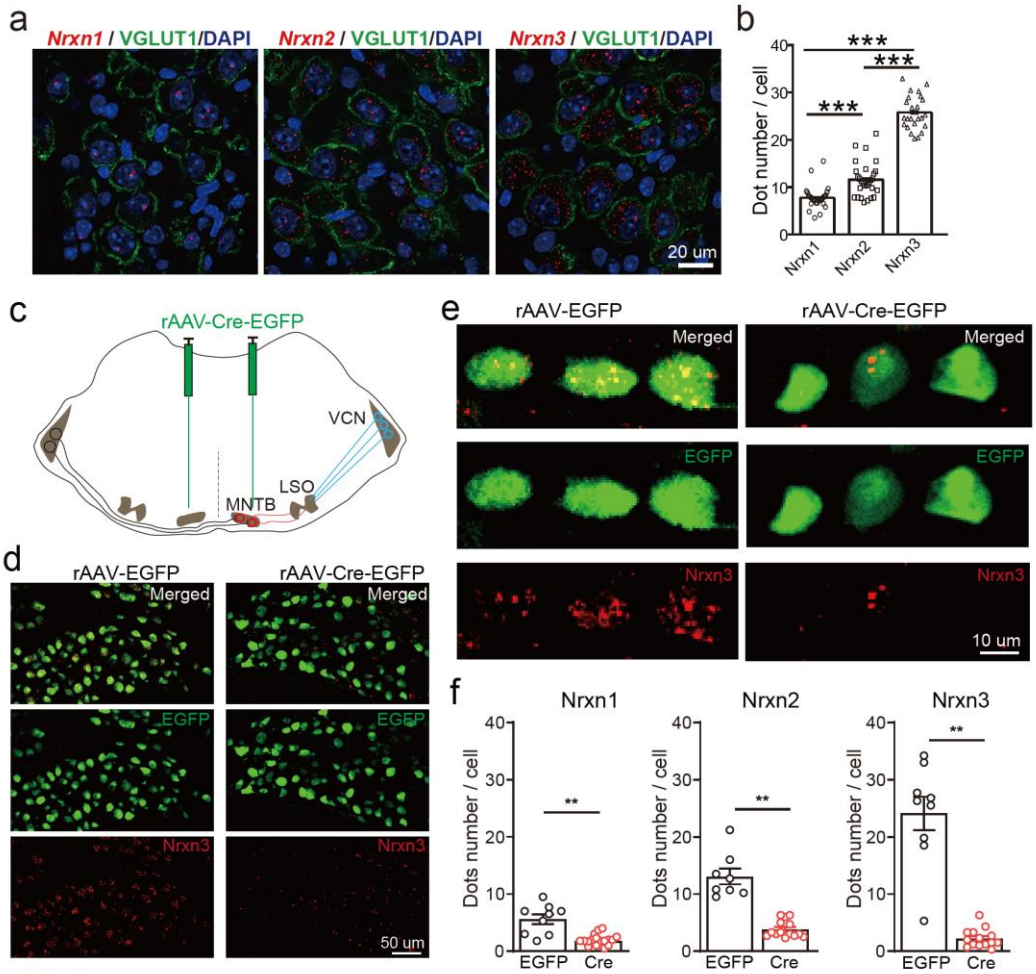

583

584

585

586 **Figure 2**

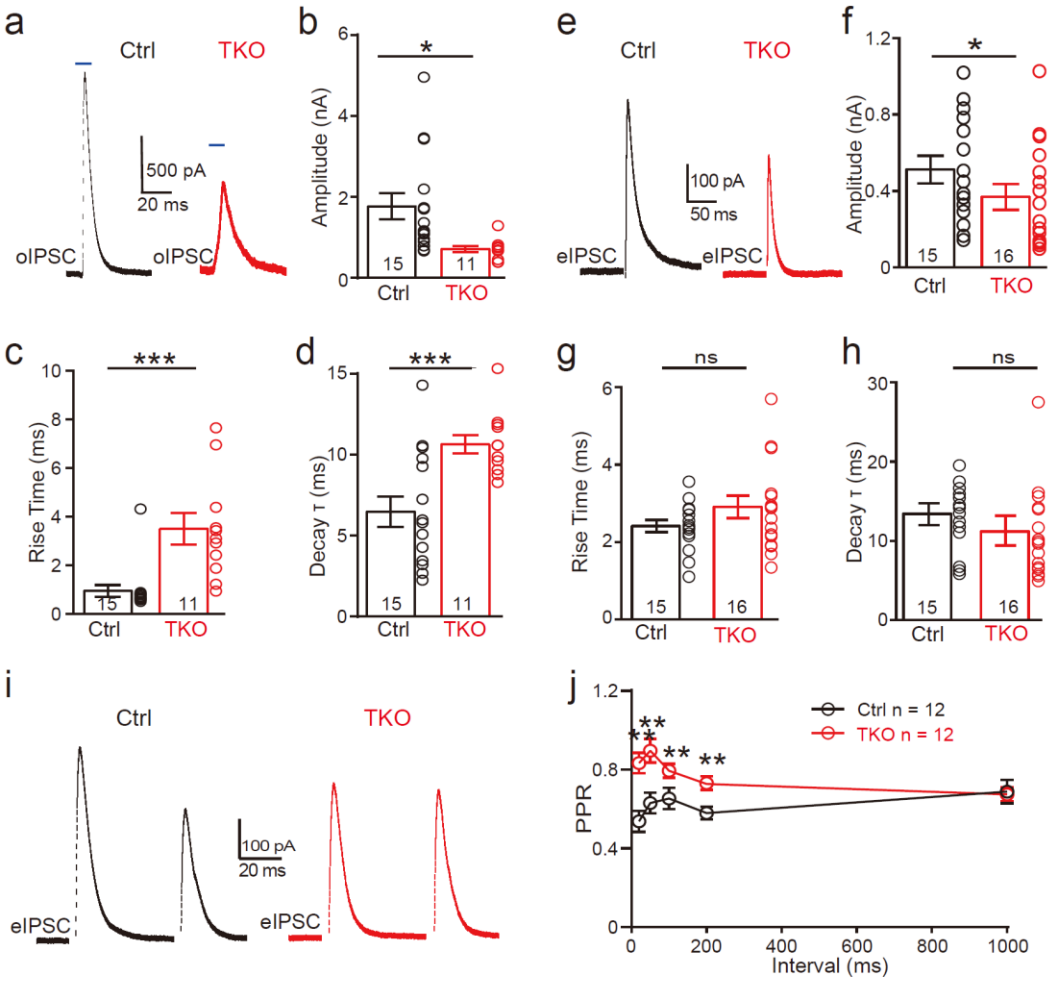

587

588

589

590

591 **Figure 3**

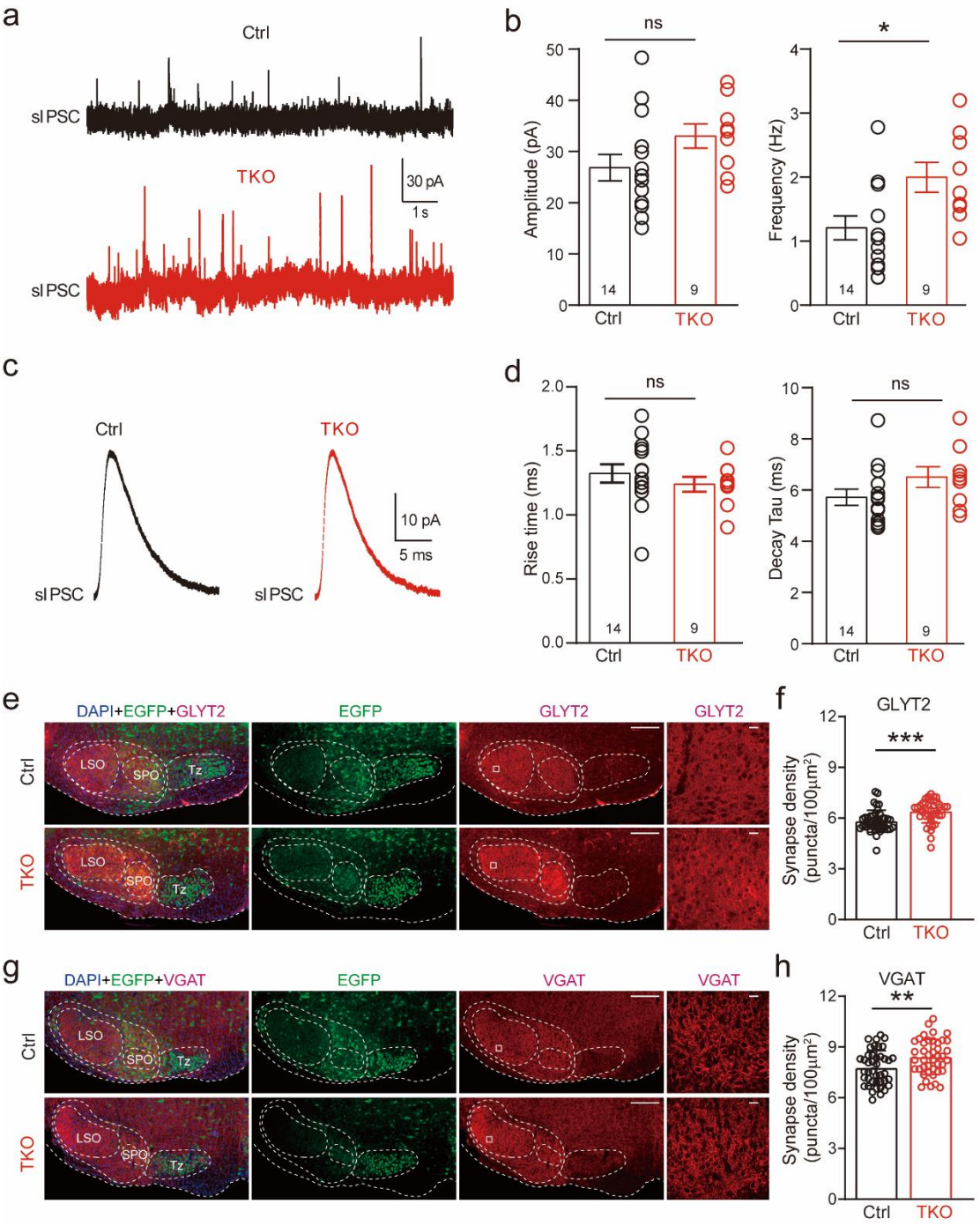

592

593

594 **Figure 4**

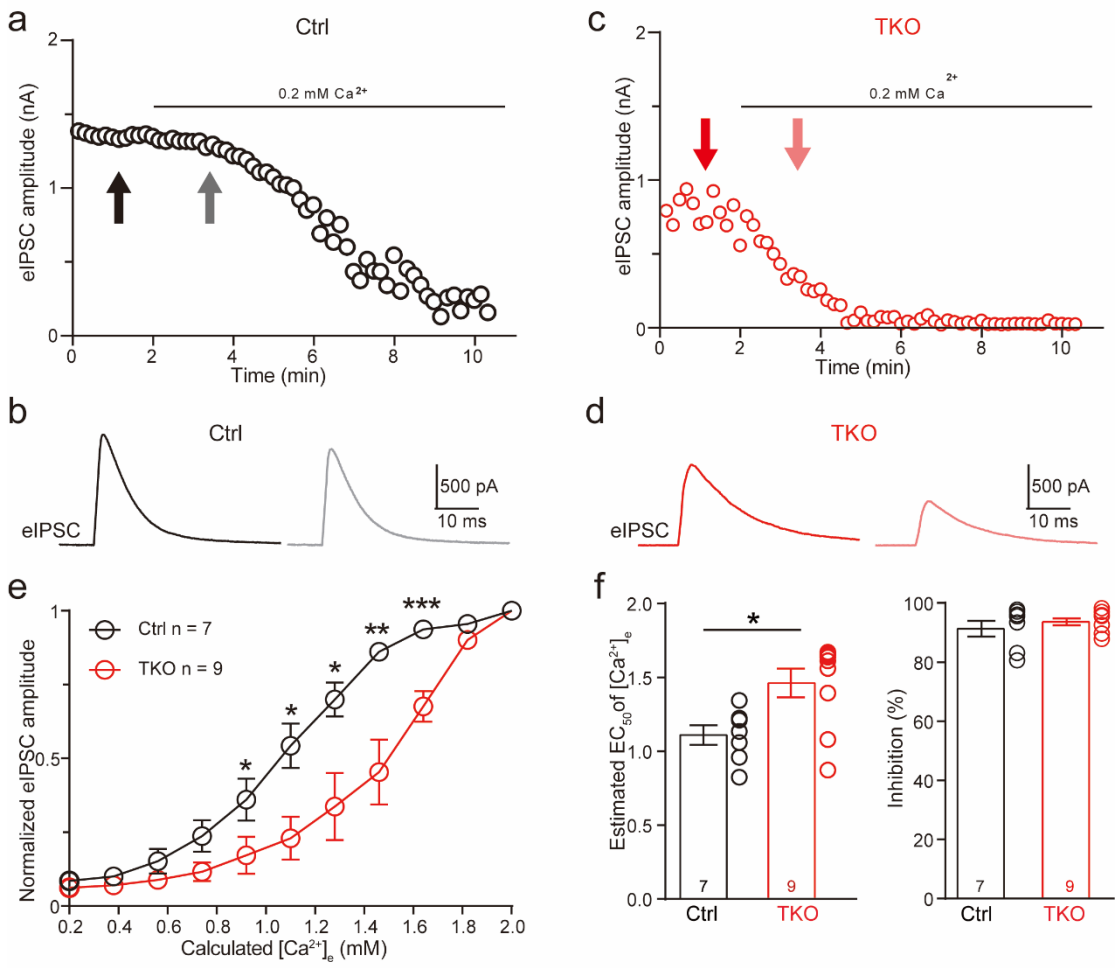

595

596

597

598 **Figure 5**

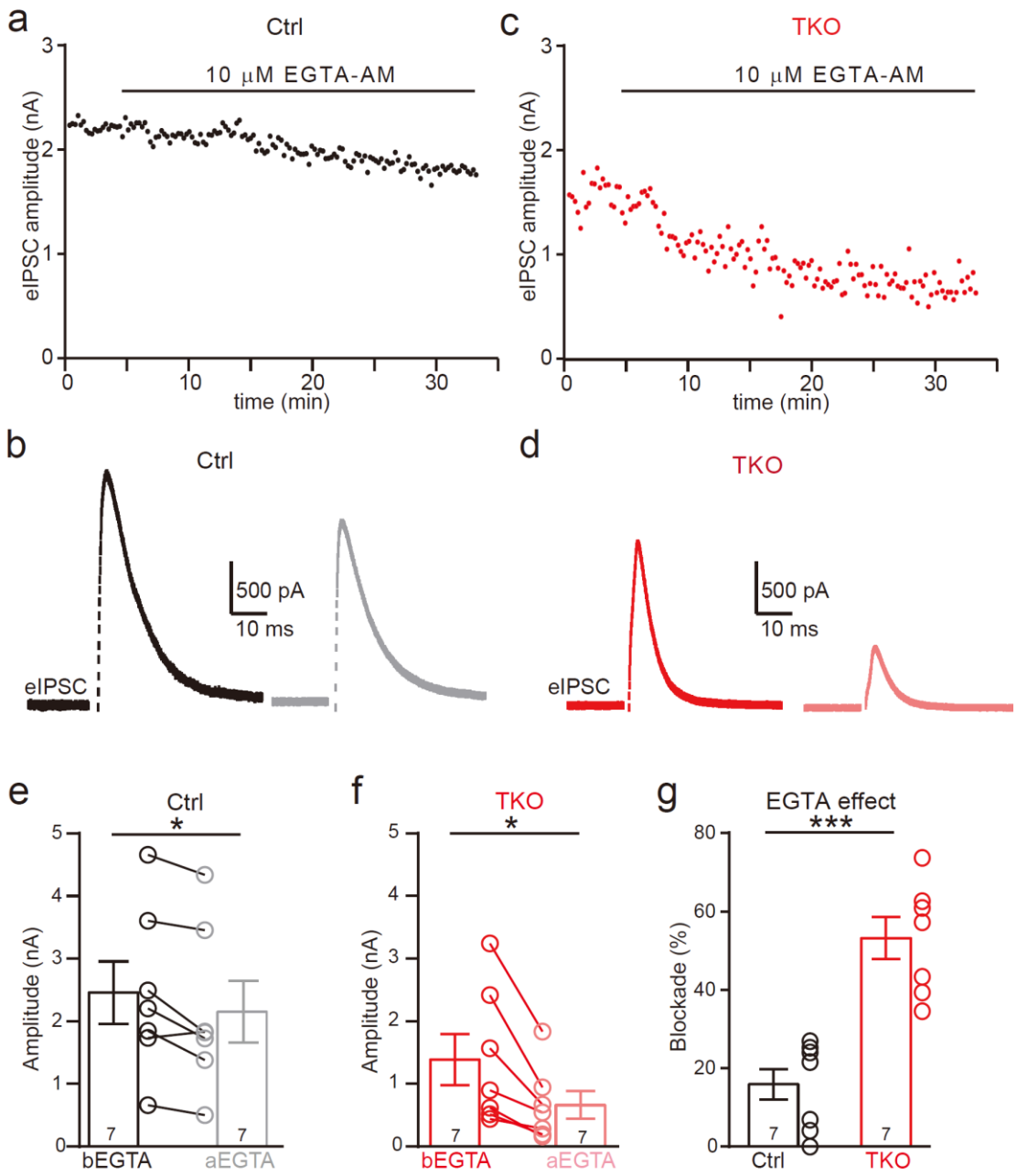

599

600

601

602

603

604

Figure S1

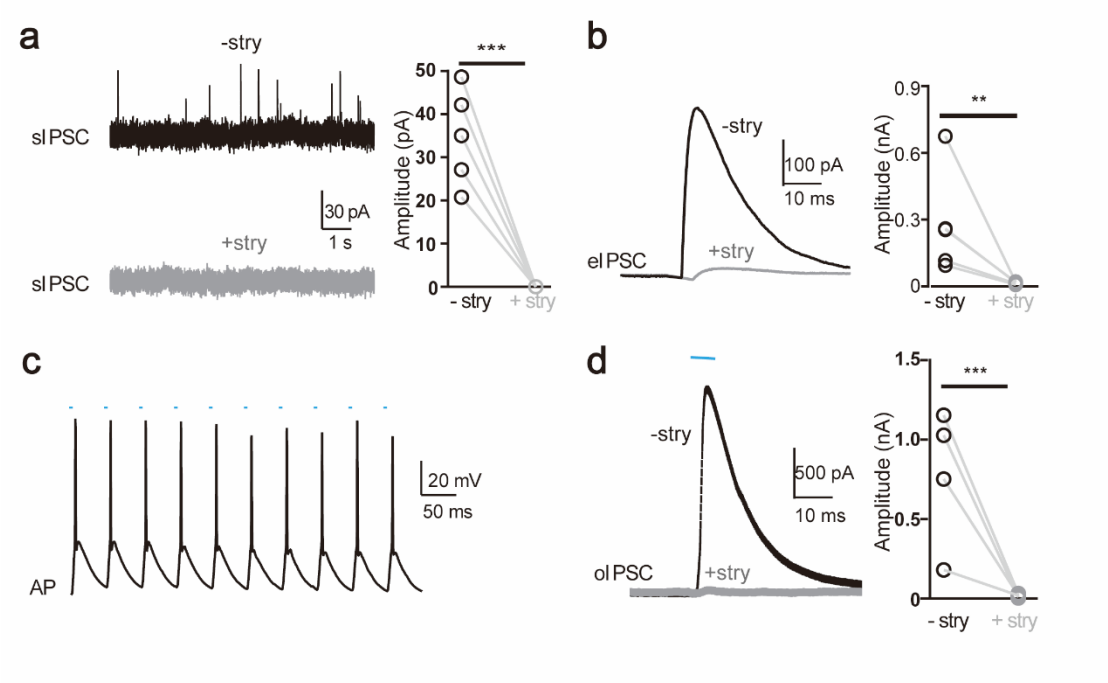

a Representative sIPSC traces of LSO neurons before and after application of potent glycine receptor blocker strychine (stry) (left) and summary of sIPSC amplitude without and with stry (right).
b Representative eIPSC traces of LSO neurons before and after stry application (left) and summary of eIPSC amplitude without and with stry (right).
c Representative action potential (AP) firing of MNTB neurons infected with ChR2 during high frequency repetitive pulse stimulation of 473 nm.
d Representative oIPSC traces of LSO neurons before and after stry application (left) and summary of oIPSC amplitude without and with stry (right).

Figure S2

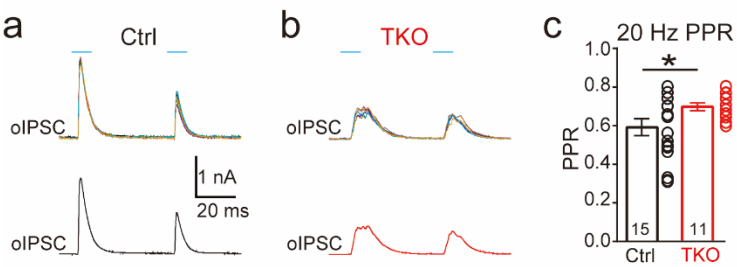

a,b Representative IPSC traces of LSO neurons evoked by paired-pulse (20 Hz) optogenetic stimulation of ChR2 expressed in MNTB neurons in control (**a**) and Nrxn TKO (**b**) mice. Top, individual trials. Bottom, averaged trace of IPSC.

607 **c** Summary of paire-pulse ratio (PPR) of IPSC amplitude.

608

Figure s3

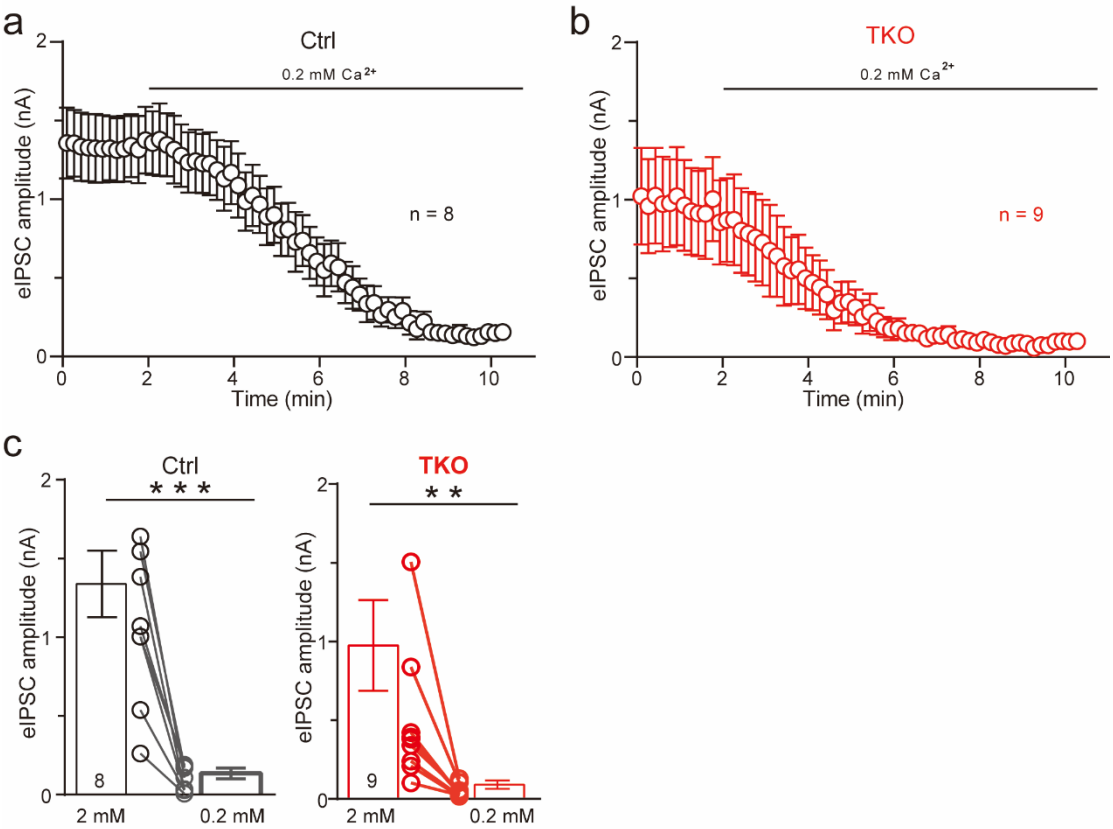

a Summary of eIPSC amplitude of control during 0.2 mM Ca^{2+} perfusion. Mean ± SEM.
b Summery of eIPSC amplitude of TKO during 0.2 mM Ca^{2+} perfusion. Mean ± SEM.
c Average of eIPSC amplitude before and after 0.2 mM Ca^{2+} perfusion. Mean ± SEM.
(**P < 0.01, ***P < 0.001), paired t-test.

Figure s4

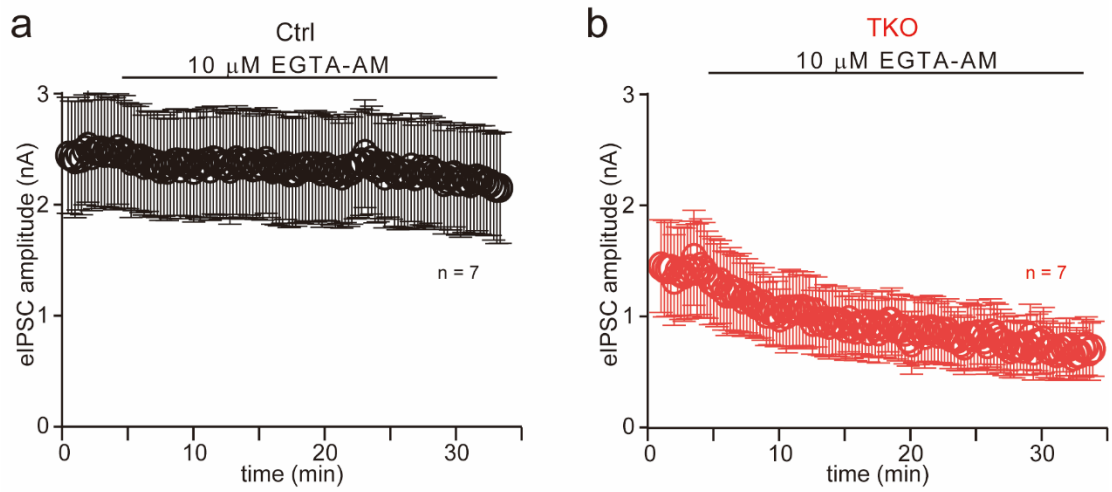

611 **a** Summary of eIPSC amplitude of control during 10 μM EGTA-AM treatment. Mean ± SEM.
b Summary of eIPSC amplitude of TKO during 10 μM EGTA-AM treatment. Mean ± SEM